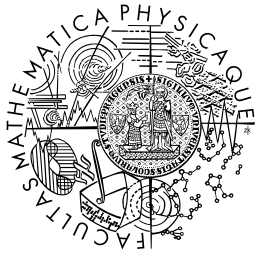

FACULTY
OF MATHEMATICS
AND PHYSICS
Charles University

BACHELOR THESIS

Michal Jireš

Simulation of rings surrounding the progenitor of SN1987A

Institute of Theoretical Physics

Supervisor of the bachelor thesis: doc. Mgr. Ondřej Pejcha, Ph.D.

Study programme: Physics

Study branch: Physics

Prague 2024

I declare that I carried out this bachelor thesis independently, and only with the cited sources, literature and other professional sources. It has not been used to obtain another or the same degree.

I understand that my work relates to the rights and obligations under the Act No. 121/2000 Sb., the Copyright Act, as amended, in particular the fact that the Charles University has the right to conclude a license agreement on the use of this work as a school work pursuant to Section 60 subsection 1 of the Copyright Act.

In ..... date ....

Author's signature

I would like to thank my supervisor Ondřej Pejcha and advisor Damien Gagnier for great guidance of this thesis and their patience.

Title: Simulation of rings surrounding the progenitor of SN1987A

Author: Michal Jireš

Institute: Institute of Theoretical Physics

Supervisor: doc. Mgr. Ondřej Pejcha, Ph.D., Institute of Theoretical Physics

Abstract: SN1987A, the first supernova visible by the naked eye since 1600s, is anomalous by existence of preexisting triple ring nebula around it. One candidate explanation of the nebula is a binary merger of SN1987A's progenitors. This was already modelled in previous work with smoothed-particle hydrodynamics code GADGET. This thesis aims to replicate this model using mesh-based hydrodynamics code Athena++ and compare it. We focus on ejected mass per latitude distribution and total ejected mass.

Keywords: SN1987A, simulation, binary merger

Contents

Introduction

Supernova SN1987A was the first supernova visible by the naked eye since 1600s unique by many properties. For us the interesting anomaly is the triple-ring nebula surrounding the supernova. Given it's non-spherical but axially symmetrical nature, one proposed explanation is binary merger of two progenitor stars.

Our goal is to create hydrodynamic simulation of the binary merger using mesh-based Athena++ resulting in ejected mass in directions of the three rings. The model is simplified, we simulate only the envelope of common envelope evolution, the binary itself is in the excised inner region and approximated by spherically symmetrical initial conditions and gravitational potential. The effects of the spiral-in on the envelope is simplified into two stages, first is slow transfer of angular momentum, and second is injection of energy corresponding to the final collision of the binary.

Similar setup was used in previous work T. Morris and Ph. Podsiadlowski 2006 and Morris and Ph Podsiadlowski 2009 using particle-based GADGET. We use the same two stages and similar initial conditions, with adjustments for static gravitational field. We will simulate subset of their parameter study including the SN1987A model specifically. We shall than compare results, mainly the amount of ejected mass in given directions.

Section 1 introduces reader to SN1987A, its progenitor and binary mergers. Section 2 introduces Athena++ hydrodynamic code and basic principles behind it, which are used for our simulation. At the end follows quick overview of GADGET for comparison. Section 3 describes specifics of our model of common envelope evolutions. Section 4 demonstrates the results gained from our simulation and compares them.

1. SN1987A and binary mergers

1.1 SN1987A

Type II Supernova SN1987A in Large Magellanic Cloud close to Milky Way was the first supernova visible to the naked eye since 1604. Its unique proximity allowed its study in great detail. It was the first case of neutrinos we measured coming from a supernova, confirming role of neutrinos in star core collapse (Philipp Podsiadlowski 1992). Most importantly for us, the supernova is surrounded by complex nebula hinting at its past.

1.1.1 Progenitor

Its progenitor was blue supergiant Sk –69°202. This on its own is unusual for Type II supernova, which were though to come from red supergiants. Since then observations of other supernovae with blue supergiant as a progenitor became more common, with 1–3 % core–collapse supernovae being photometrically similar (McCray and Fransson 2016). Still, good progenitor model must be able to explain this anomaly.

1.1.2 Nebula

The supernova is surrounded by low-density complex axisymmetric nebula, whose 3D structure was measured from echoes of the supernova bouncing of the surrounding gas (Sugerman et al. 2005). The major high-density features of the full nebula is easily visible triple-ring nebula consisting of 3 axisymmetric rings, bright equatorial ring and two dimmer rings north and south. Sizes and speeds of these ring suggest that these rings are result of single astronomical event in near past, 10'000s years ago.

Figure 1.1: Rings of SN1987A taken by Hubble Space Telescope. (NASA, ESA, and R. Kirshner (Harvard-Smithsonian Center for Astrophysics and Gordon and Betty Moore Foundation) and P. Challis (Harvard-Smithsonian Center for Astrophysics) 2017)

1.2 Possible models explaining anomalies

Philipp Podsiadlowski 1992 explored anomalies of SN1987A and possible explanations, in short the main anomalies are:

- Compactness of the progenitor, Type II supernova are expected be result of red supergiants, instead of relatively compact blue supergiant
- The surrounding nebula and its axisymmetricity, likely result of rapid rotation flattening the envelope
- Chemical anomalies in both progenitor and the rings, they both contain excess of s-process elements in the otherwise hydrogen-rich envelope

No single model so far can explain all these anomalies. Main problem lies with the chemical anomalies. However models which can explain the most anomalies are binary models: accretion and merger models. In this paper we focus on the merger model.

1.3 Binary mergers

1.3.1 Common Envelope

Many stars exist in close binaries. As one star ages and increases volume of its envelope, in close binary system it may overflow its Roche lobe and start mass transfer to the other star (Metzger and Pejcha 2017). With the mass transfer the other star may overflow its Roche lobe as well, creating common envelope that is not bound to either star on its own.

Stars in the common envelope will experience drag from the surrounding envelope gas, slowing down the stars and causing them to spiral in. Which continues until the stars' cores merge. Alternatively one of them may explode earlier due to accretion, which may be another possible explanation of SN1987A's rings. We focus on the merger model.

As the stars spiral inwards, they have to get rid of excess angular momentum and kinetic energy into the surrounding envelope. The angular momentum is transferred slowly during the whole spiral-in. The kinetic energy dissipated during the early spiral-in is minimal, most of the kinetic energy is transferred in the last stages of the spiral-in (T. Morris and Ph. Podsiadlowski 2007).

We can thus model the spiral-in transfer as firstly only transfer of angular momentum. This happens slowly and so the angular momentum spreads over the whole envelope to form flattened envelope. Then during the core merger there is fast injection of energy into inner regions of the envelope.

1.3.2 Ejection of envelope

The energy is injected into the envelope near its core. Since the envelope is flattened, the shock has easier path to outside of the envelope in the polar region. Once it reaches the edge, the energy of the shock ejects some of the envelope's mass.

In the equatorial region, there is much more mass in the way which dissipates the energy of the shock, leaving (almost) no remaining energy once the shock reaches the edge of the envelope.

At the border of these two extremes, there are latitudes where the mass will be already ejected outside of the envelope, but additional ejected mass can be added from neighboring envelope. We would then expect that at such latitude we would observe density peak, which could explain the non-equatorial rings of SN1987A.

In cases with larger injection of energy, the shocks may not be dissipated through the equatorial region and will reach the farthest edge of the envelope. Since the outer regions of envelope are already loosely bound, this would result in mass ejection of equatorial region as well. Though the equatorial ring of SN1987A is expected to be result of later processes (T. Morris and Ph. Podsiadlowski 2006).

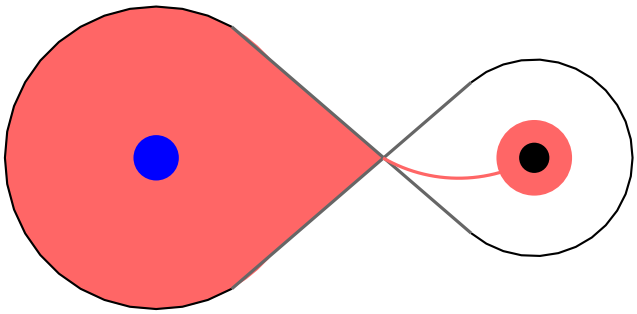

(a) Overflow of Roche lobe.

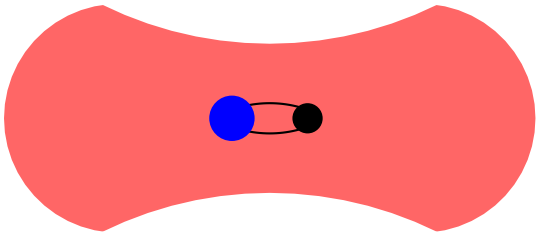

(b) Binary spirals in, sharing the envelope.

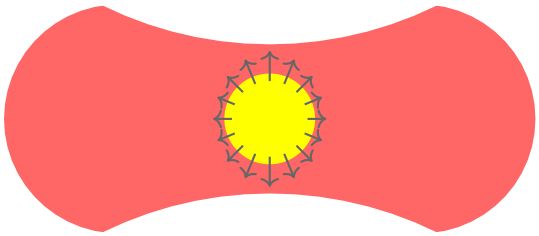

(c) Binary merger, partially ejecting the envelope.

Figure 1.2: Common envelope evolution of binary merger.

2. Hydrodynamic codes, Athena++

2.1 Hydrodynamic equations

To simulate the evolution of binary merger, we will represent the envelope as a fluid. We need to solve the equations of hydrodynamics, expressing conservations of mass, linear momentum and energy:

$$\frac{\partial \rho}{\partial t} + \boldsymbol{\nabla} \cdot \rho \mathbf{v} = 0 \tag{2.1}$$

$$\frac{\partial \rho \mathbf{v}}{\partial t} + \boldsymbol{\nabla} \cdot (\rho \mathbf{v}\mathbf{v} + P\mathbf{I} + \mathbf{T}) = -\rho \boldsymbol{\nabla} \Phi \tag{2.2}$$

$$\frac{\partial E}{\partial t} + \boldsymbol{\nabla} \cdot ((E + P)\mathbf{v} + \mathbf{T} \cdot \mathbf{v}) = -\rho \mathbf{v} \cdot \boldsymbol{\nabla} \Phi \tag{2.3}$$

The energy density E is related to internal energy density e as $E = e + \frac{1}{2}\rho \mathbf{v}^2$. Pressure P can be expressed as $P = (\Gamma - 1)e$. $\Gamma = \frac{5}{3}$ is the adiabatic index. $\mathbf{T}$ is the viscous stress tensor, which will be zero because our model will not contain viscosity. Φ is the gravitational potential, we will be using point mass potential:

$$\Phi = -\frac{GM}{r} \tag{2.4}$$

2.2 Athena++

Athena++ (Stone et al. 2020), is mesh–based magneto-hydrodynamic code. It supports complicated mesh refinements, however we will be using a simple grid in spherical coordinates with pure hydrodynamics.

In Athena++ the simulation is represented by grid of cells spanning the whole simulated region. Each cell is defined by intervals in the 3 spacial coordinates, resulting in cubes in Cartesian coordinates, and cube-like volume in spherical coordinates. Each cell contains single value for each of conserved values: mass, energy and linear momentum in each spacial direction. The values are normalized by volume of the cell.

In our case of simple spherical grid the cells are uniformly distributed for the angular coordinates. For the radial direction, size of the cells is exponential, each following cell is x-times longer than previous, $x = 1.004$ in our case. Inner region of the spherical grid will have smaller cells than outer regions. Otherwise if the radial direction would be uniform as well, the ratio of cell length and width would vary drastically, because width in angular coordinates depends on distance from center.

The whole grid is updated in a uniform timestep. During this step, new values are computed from previous values of any given cell and its neighbours using a Riemann solver. The length of the timestep is limited by sizes and velocities of cells. Because each cell is updated only from its neighbours, no mass can cross

the entire cell during a single timestep. This way we come to the upper limit on timestep length τ:

$$\text{For all cells: } \forall i : \tau \leq \frac{d_i}{v_i} \tag{2.5}$$

where $i \in 1, 2, 3$ is a index of a coordinate, d_i and v_i are cell width and velocity of a cell in given coordinate.

To improve stability, the timestep is further limited by a constant CFL number, which we set to $C = 0.5$:

$$\text{For all cells: } \forall i : \tau \leq C\frac{d_i}{v_i} \tag{2.6}$$

2.2.1 Polar averaging

Limitation of timesteps based of dimensions of cells works well with uniform grids. However with spherical grid the cells in polar region are squished along azimuthal direction. Thus even if the velocities in polar cells are smaller than velocities in equatorial region, they still limit timesteps to a magnitude smaller, simply because polar cells are smaller.

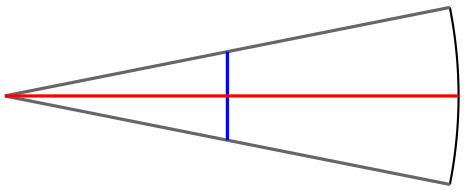

Figure 2.1: In polar region, width of azimuthal direction (blue) is relatively small, as opposed to latitudinal direction in red, leading to small cross times.

Since we are not interested in polar region, we can increase timesteps by unifying polar cells along azimuthal coordinate into several larger cells. This is not directly possible in upstream version of Athena++, but we use modification implemented by my advisor Damien Gagnier (Gagnier and Pejcha 2023). It does not unify directly, but after each step it averages values along the conceptually unified cells. Given that the problem is almost symmetrical, the cells should have similar values, and the averaging should not have any effect outside of larger possible timesteps.

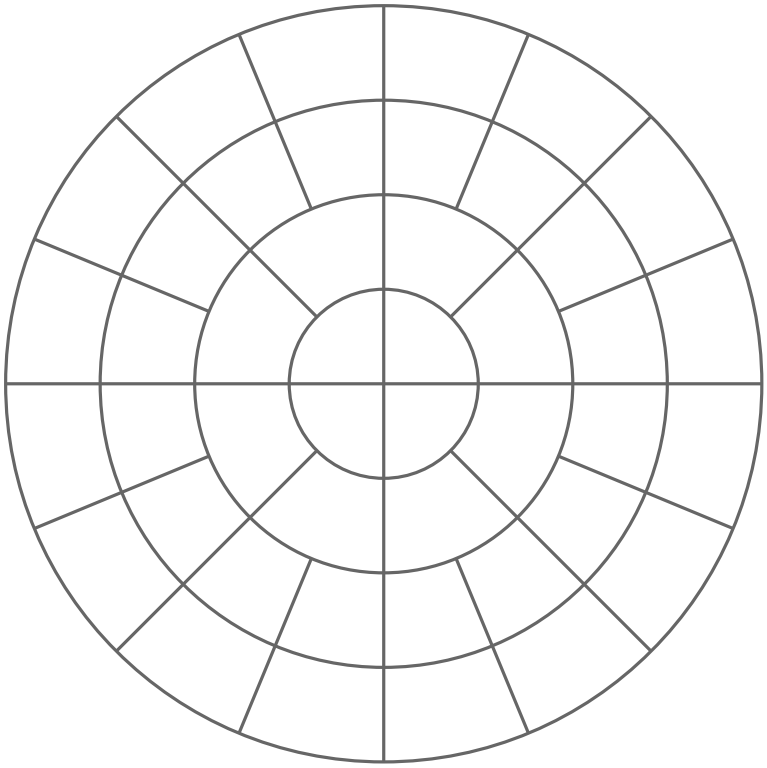

Figure 2.2: Polar averaging/unifying to increase width of azimuthal direction of polar cells.

2.2.2 Simulation

The whole grid is divided into blocks, typically each block contains 64x64x64 cells. Each block, for a single timestep, can be computed independently. This allows the computation to be distributed across multiple threads/computers using OpenMPI. Each thread gets at least one block. Because the updates are local, only the boundary cells must be shared after each update.

Each block contains two layers of boundary ghost cells in each coordinate direction. Ghost cells are not modified directly by the update, but their values are used to update cells which would otherwise lack neighbours. They convey information about the outside region. If the outside region is another block, ghost cells contain copy of boundary cells in the other block. If the outside region is outside of the whole simulated region, then the ghost cells are set to fulfill a boundary condition.

2.3 Riemann Problem

Single dimensional Riemann problem (Toro 2009) is characterized by two regions, each with uniform initial conditions, divided by single discontinuity. The solution contains several moving points of discontinuity, called shocks. Simplest example is the shock tube problem, where initially the two regions differ by density.

In our simulation Riemann problem corresponds to two cells next to each other, where the discontinuity separates them.

2.3.1 Riemann Solvers

If the hydrodynamic equations are linear we can solve the problem exactly. In general, the hydrodynamic equations are not linear, and thus we have to approximate.

There are several Riemann solvers such as Roe, HLLE, HLLC, each approximating differently, resulting in different properties. We used the default solver in Athena++ HLLC.

2.4 Alternative code – GADGET

GADGET (Springel 2005) is code supporting hydrodynamic simulations using smoothed-particle hydrodynamics. It is used for papers T. Morris and Ph. Podsiadlowski 2006 and Morris and Ph Podsiadlowski 2009 which we try to replicate using Athena++.

GADGET's particles have a smoothing radii, each particle interacts with particles inside the radii. The smoothing radius is updated to contain almost constant number of neighbours. From the radius and particles inside it, the local density and pressure are computed. The pressures are then used to determine acceleration of the corresponding particle.

Differences:
GADGET:

- Self-gravity: One of GADGET's purposes is to simulate interacting galaxies, it thus supports self-gravity, gravity caused by the particles themselves, using tree data structures for approximation of distant regions.
- GADGET's particles can move arbitrarily far, not limited by a simulated region.
- Particles have minimal mass, decreasing this mass leads to more particles, which are computationally expensive.
- Introduces artificial viscosity that would not exist in real system.

Athena++:

- Arbitrarily big ratio of densities. Each cell can have almost arbitrarily small or big density.
- Ghost cells allow easy boundary conditions.
- Uses Riemann solvers which can more accurately simulate shock fronts.
- Missing self-gravity in spherical coordinates. We have to use gravitational potential of a single point mass.
- Limited to the simulated region. Increasing the region size, while keeping the resolution constant is computationally expensive.

3. Model

We are simulating simplified model of binary merger inside of common envelope. We simulate only the envelope, the binary itself is in the excised inner region of spherical coordinates. The initial conditions and gravitational potential are spherically symmetrical.

The simulation is conceptually divided into two active phases:

- Spin-up - during first phase we slowly increase the angular momentum of the envelope, excluding the outer regions that exceed local keplerian velocity. This corresponds to the slow transfer of angular momentum over the whole spiral-in.
- Energy injection - during short second phase, we in single step inject energy into inner cells right above the excised region. This corresponds to the final collision of binary which we approximate as instantaneous.
- Observation - after previous active phases we simulate and observe until the distribution of ejected mass stabilizes.

These steps and initial conditions are taken from T. Morris and Ph. Podsiadlowski 2006, which we compare to. Unlike them we approximate the gravitational potential as result of single point mass with 20 solar masses .The gravitational potential is greater in inner regions, however the outer regions we are most interested in should not be affected much by the difference to self–gravity. Unfortunately Athena++, unlike GADGET, does not support self-gravity (dynamic gravity field caused by particles themselves) in spherical coordinates.

We expect (1.3.2) that the energy injection will cause shocks that will propagate through the envelope and cause ejection of mass in direction of non-equatorial rings. The equatorial ring can be explained by later solar wind of the blue giant, which is not part of this simulation (T. Morris and Ph. Podsiadlowski 2006).

3.1 Shared parameters of models

Chosen units of mass, distance and time of the simulation are $M_\odot$, $R = 1500R_\odot$ and a year respectively. Where R is the radius of initial envelope.

Initial masses of the stars are $15M_\odot$ and $5M_\odot$, with initial distance $2500R_\odot$ in case of SN1987A. However we simulate only the envelope. The excised inner region corresponding to the core contains $8M_\odot$. The simulated region corresponding to the envelope contains $12M_\odot$.

The excised inner region corresponding to the core covers radii $r < \frac{1}{10}R$ and is assumed to have a reflecting surface not allowing for mass transfer. The simulated region containing the envelope covers radii between $\frac{1}{10}R < r < 20R$.

The gravitational potential is static and is modelled with point mass in coordinate center representing total mass of the system $20M_\odot$.

All specified years in figures are specified after the energy injection.

3.2 Initial Conditions of the common envelope

We start the common envelope with stable spherically symmetrical conditions, with adiabatic index of the gas $\Gamma = 5/3$.

Stable spherically symmetrical conditions must fulfill following equations:

$$\frac{\mathrm{d}P}{\mathrm{d}r} = -\rho\frac{\mathrm{d}\Phi}{\mathrm{d}r} \qquad P = K\rho^{\Gamma} \tag{3.1}$$

Where K is a constant.

Fitting density profile is modified from Gagnier and Pejcha 2023:

$$\frac{\rho(r)}{\rho(r_{in})} = \left(1 + (\kappa - 1)\frac{\frac{1}{r} - \frac{1}{r_{in}}}{\frac{1}{R} - \frac{1}{r_{in}}}\right)^{n} \tag{3.2}$$

$$K = \frac{GM}{(n+1)\rho(r_{in})^{\frac{1}{n}}(\kappa - 1)}\left(\frac{1}{R} - \frac{1}{r_{in}}\right) \tag{3.3}$$

Where $\kappa^n = \frac{\rho(R)}{\rho(r_{in})}$ specifies ratio of densities on the surface of the inner region and surface of the envelope, R is the envelope radius, r_{in} is the radius of excised region

Outside of the envelope the density is set to minimum. The density profile is modified by random seed perturbations of $\pm 0.1\%$, to dissipate waves that would otherwise appear and persist with fully axially symmetrical initial conditions.

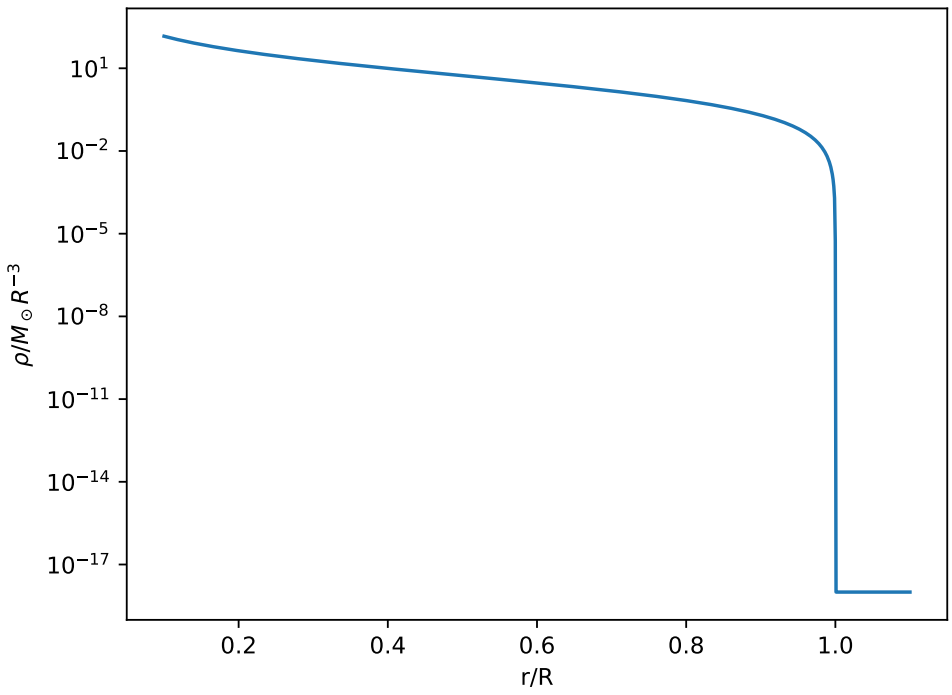

Figure 3.1: Initial distribution of density.

3.3 Parameter study

To consider the validity of the model, and to compare with T. Morris and Ph. Podsiadlowski 2006, we evaluate the model with several different angular momentums and injected energies.

Since we are using the exact same values of angular momentum and injected energy, we will use the same dimensionless constants α for injected energy and β for angular momentum. Even though they do not have a special meaning in our units.

We spin-up using two angular momentums used in T. Morris and Ph. Podsiadlowski 2006. $\beta = 0.817$ is momentum corresponding to SN1987A modelled with star masses $M_1 = 8M_\odot$ and $M_2 = 12M_\odot$ and initial orbital period of 10 years.

β	0.588	0.817
L	8.360	11.616

Table 3.1: Transfered angular momemtum in our models. Angular momentum expressed in units of the simulation ($M_\odot 1500^2 R_\odot^2 \cdot year^{-1}$).

The energies are expressed as ratio α to binding energy, but because we do not have self–gravity we cannot directly translate this ratio, because our binding energy is around twice as much. We assume that ejected mass is proportional to the binding energy of outer regions of the envelope, and thus mostly unaffected by self–gravity. Thus for α ratios we do not use our total binding energy, but we use the binding energy of corresponding envelope with self–gravity in T. Morris and Ph. Podsiadlowski 2006.

α \ β	0.588	0.817
0.25	6.17	5.14
0.33	8.15	6.79
0.40	9.88	8.23
0.50	12.35	10.29

Table 3.2: Injected energies in the simulation's units ($M_\odot 1500^2 R_\odot^2 \cdot year^{-2}$).

Unlike T. Morris and Ph. Podsiadlowski 2006, we consider only the case when the energy is injected directly after the spin–up.

3.4 Spin-up

All angular momentum contained in the original binary will be transferred into the envelope. For point masses orbiting on circular orbits, we get:

$$L = \frac{M_1 M_2}{(M_1 + M_2)^{\frac{1}{2}}} R^{\frac{1}{2}} G^{\frac{1}{2}} \tag{3.4}$$

Where M_1 and M_2 correspond to their initial masses, and R is their initial distance.

Interestingly, while the T. Morris and Ph. Podsiadlowski 2007 paper uses identical expression, G is already expanded with units claimed to correspond to $M_1 = M_5 = 5M_\odot$, $M_2 = M_{15} = 15M_\odot$, $R = A_{2500} = 2500R_\odot$. However the expanded value of G corresponds to values $M_5 = 8M_\odot$ and $M_{15} = 12M_\odot$ which are masses of central mass and envelope mass. This value for angular momentum of SN1987A is then also used in their other papers. While we note this discrepancy, we will use angular momentum used in the T. Morris and Ph. Podsiadlowski 2006 paper so that we can compare results.

During spin-up we increase azimuthal velocity of each cell by constant angular acceleration $\frac{\mathrm{d}\omega}{\mathrm{d}t} = 1$, $\Delta v_\phi = \Delta\omega r$. The acceleration is not applied to cells whose total velocity already exceeds local keplerian velocity. We want to prevent adding angular momentum into parts of envelope that are already escaping, which have no physical reason to gain so much additional angular momentum.

$$\Delta v_\varphi = \begin{cases} r\Delta\omega = r\Delta t & \text{if } |v| < \sqrt{GM} \\ 0 & \text{otherwise} \end{cases} \tag{3.5}$$

This will leave us with inner envelope orbiting with the same angular velocity, and outer envelope limited by local keplerian velocity. This spin-up procedure mirrors the spin-up in T. Morris and Ph. Podsiadlowski 2006 applied to mesh based code. It is common to spin-up limited only by azimuthal velocity, however this leads to outer parts of envelope reaching escape velocity.

Spin-up without self-gravity is slower. Without self-gravity, more mass in initial conditions is concentrated in lower radii. Thus even when our angular acceleration is larger than in T. Morris and Ph. Podsiadlowski 2006, it will take longer time to add same amount of angular momentum. Our main goal is to add angular momentum in quasi-stable manner, secondarily we want to achieve similar envelope shapes.

The achieved envelope shapes (Figure 3.2) closely mirror the ones in T. Morris and Ph. Podsiadlowski 2006, though the envelope is less flat – our maximum $\sim 1.6R$ half-width vs their $\sim 1.2R$. Which might be caused by the lack of self-gravity.

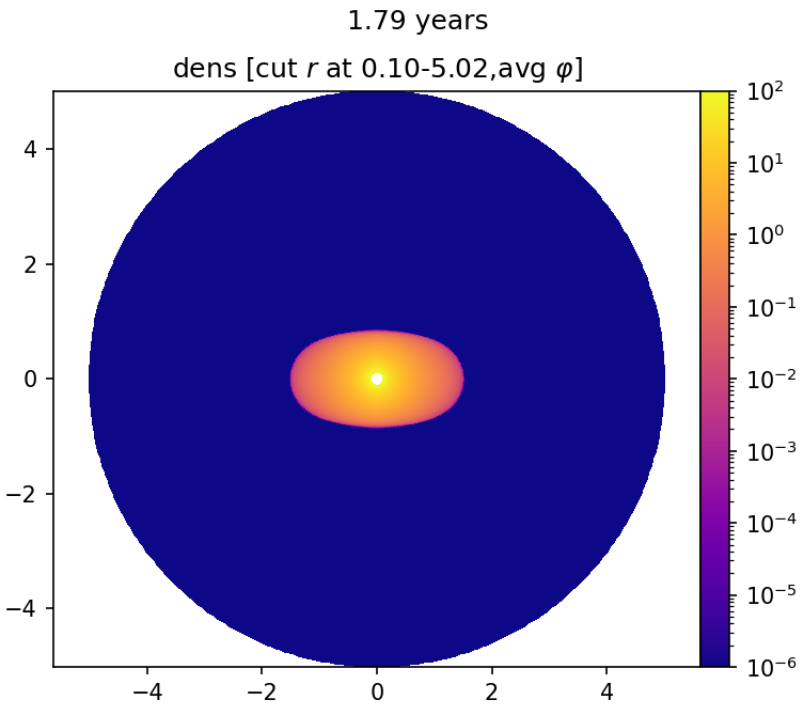

(a) $\beta = 0.235$

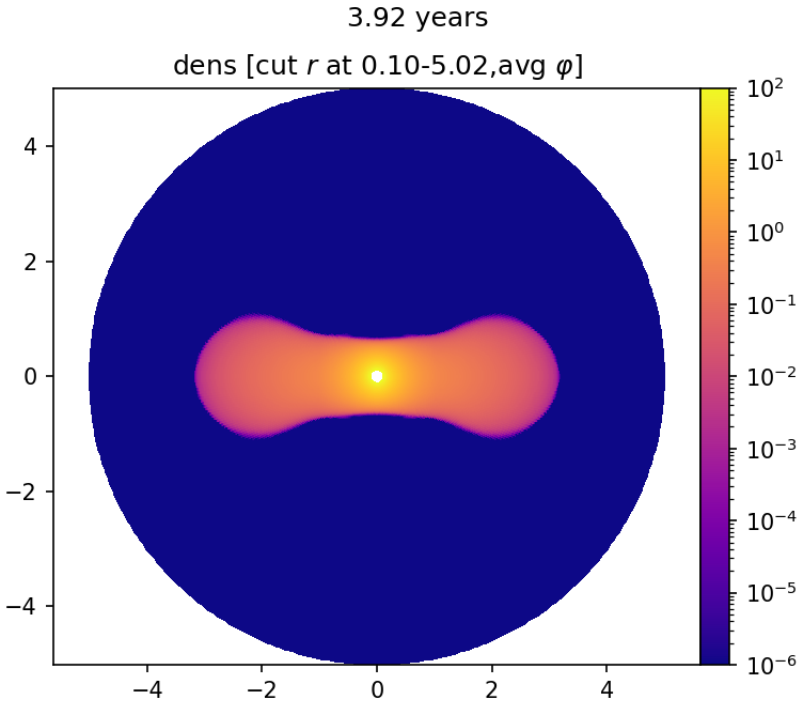

(b) $\beta = 0.588$

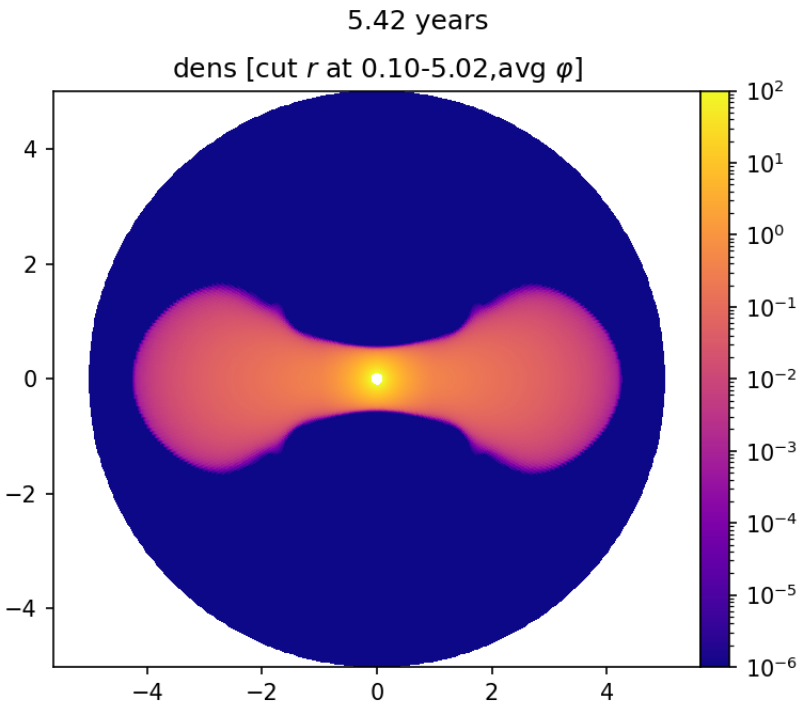

(c) $\beta = 0.817$

Figure 3.2: Shapes of envelopes (density distribution) after spin-up, corresponding to values used in T. Morris and Ph. Podsiadlowski 2006, in this paper we use only the last two. Specified years correspond to how long was the spin-up.

3.5 Injection of energy

Injection of energy follows directly after spin-up. The energy is injected in inner region with $r < 2/15R$. Even though large part of this region is cut out of our model, this region still contains more mass than in T. Morris and Ph. Podsiadlowski 2006 because of different stable solution (initial conditions) without self-gravity. The energy is distributed proportionally to mass.

3.6 Observation

3.6.1 Ejected mass

Mass of a cell is considered to be ejected, if it has energy to escape the gravitational potential and thus unbound. There are several ways how to decide whether mass in unbound. However given the dominance by radial kinetic energy, the measure of ejected mass is mostly equivalent to alternative measurements of ejected mass. This may be inaccurate in early stages of energy deposition when the path is obstructed my non escaping cells, but later they are different only by a single layer of cells, once the escaping mass is not obstructed. For easiest computation we use $E + E_p$, the energy of the cell as simulated by Athena++ with added

potential energy. Mass that escaped the simulated region is considered ejected as well, with assumption for simplicity that its polar angle θ is constant.

3.7 Model details

We have chosen spherical coordinates with resolution 768 for radial, 256 for azimuthal, and 192 for polar coordinate. The azimuthal angle resolution is reduced in ratio to polar angle resolution, because the problem is almost azimuthally symmetrical, and thus the minor differences are due to initial perturbations, and we can sacrifice these details which should not influence the global picture.

For polar angle and radial resolutions we try to create cells with squarish proportions, this is clearly unachievable to do in spherical coordinates with uniform division of dimensions. Thus we use grid ratio of 1.004 for radial direction - which means that cells intervals in radial direction can be described using $r_{j+1} - r_j = 1.004(r_j - r_{j-1})$. This results in ratios of roughly 1:1 at the original surface, 1:2 at the inner boundary and at the envelope boundary, and 1:3 at the outer boundary which we consider close enough.

Details of exact settings can be seen in Athena++'s input file supplied in Attachment A.3. Athena++'s problem generator for this model is supplied in Attachment A.2, which describes initial conditions and implements spinning up and energy injection.

We modified Athena++'s code in several way, as can be seen in patch files in Attachment A.1. We use Athena++ version from February 3rd 2023 (specifically commit f16e877a35db84615d50e75db40fe066f3867ec7) as base code. These modifications include the polar averaging, and ability to save/end simulation at specific time – used for images at time of energy injection.

3.7.1 Boundary conditions

Inner boundary is reflective. No mass can pass through, into the excised inner region. Outer boundary is outflowing so that the ejected mass can freely pass to region outside of the simulation.

3.8 Numerical Instabilities

The combination of our initial conditions and longer timesteps achieved with polar averaging can result in numerical instabilities.

3.8.1 Spin-up instability

Specifically in our simulations during spin-up we encountered cells with minimal density but with total momentum in magnitude of neighboring cells. As far as we know, no cells contained physically impossible values, and their minimal density makes them inconsequential to validity of any results. However this instability causes two problems:

- The cell has large velocity and so crossing time across the cell is very small. Since the simulation is limited by crossing time, following timesteps can be

several orders of magnitude smaller than previous. In the better case, these shorter steps stabilize the instability into normal values.

- In the worse case, following steps result in NaN, which propagate through the whole simulation and ruin any useful values.

There are several possible causes and corresponding solutions:

- Our initial conditions as shown in Figure 3.1 contain sharp decrease of density at the star's surface and then set density outside to minimal floor density. All the spin-up instabilities appear at this density boundary.

  This could be rectified by adding stellar atmosphere which would make the density decrease slower. Though its mass should be negligible to the mass of the star. We tried to introduce atmosphere which would decrease exponentially from some small, but large above floor density, value of density of original initial conditions. However the amounts we introduced were insufficient. For the few values we tried, there were still occasional instabilities, only more unreliable. Thus we moved on to find more reliable solution.

- Second possible culprit is the implementation of spin-up itself. Angular momentum is added as a source term throughout the whole envelope, including cells neighboring the unstable cells. However the instability still occurs even if we disable source terms of angular momentum for ~ 10 steps before the instability. Thus we concluded that it is unlikely to be caused directly by the spin-up via some local anomaly, which would quickly disappear. Instead it is likely causes by global distribution of mass / angular momentum.

- Third possible solution is to change numerical methods to more stable variant. This however has direct negative of increased time complexity to compute and thus slower simulation.

  In our case we replaced the default ODE integrator vl2 with integrator rk3. It is roughly 50% slower, but we also increased CFL number from 0.3 to 0.5, which in total keeps the run-time just a bit slower. With this change we never encountered numerical instabilities during spin-up.

3.8.2 Expansion instability

Later we encountered second numerical instability resulting in NaN in the last stage of observation. This instability happened in polar region, thousands of simulation steps / few years after the injection of energy – the last applied source term.

Unfortunately we discovered this instability too late and had not enough time to debug it, find reliable solution, and rerun the simulation in reasonable time. Thus we are missing results for one combination of parameters.

Since no source terms were applied for long time before the instability, we assume that the reason for instability is similar to the spin-up instability, and it does not influence the validity of other simulations as long as contagious NaNs are avoided.

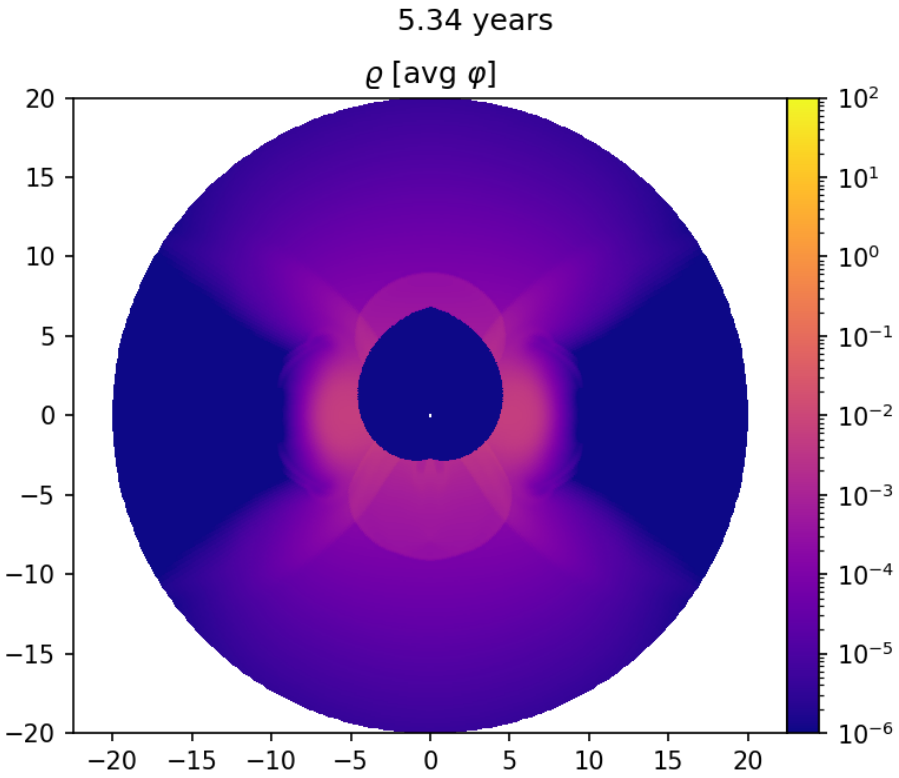

Figure 3.3: Propagation of NaNs through the simulated region.

4. Results

Figure 4.1 shows final ejected mass for each model. All specified years in figures are specified after the energy injection. In comparison to T. Morris and Ph. Podsiadlowski 2006, our model predicts ejection of mass further from the equator, above 45° while they predict angles bellow 45°. This may be influenced by the lack of self–gravity and resulting less flat spun-up envelope.

Unlike them we predict peaks even for lower energies, though still muted. The exact energies do not influence the ejection peak, only the amount of mass ejected.

We predict mass ejection in the equatorial region for the same simulations – this is not directly relevant to the non-equatorial rings, however it suggests we have chosen correct corresponding amount of energy in our model without self-gravity.

Interestingly, the ejected mass is not fully symmetrical in north and south hemisphere. This is clearly visible at peaks of $\alpha = 0.5$, $\beta = 0.588$.

Unfortunately simulation ($\alpha = 0.40$, $\beta = 0.588$) could not be finished in time because of encountered numerical instabilities (see 3.8.2).

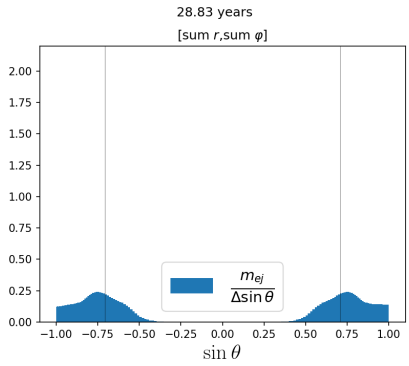

(a) $\alpha = 0.25$, $\beta = 0.588$

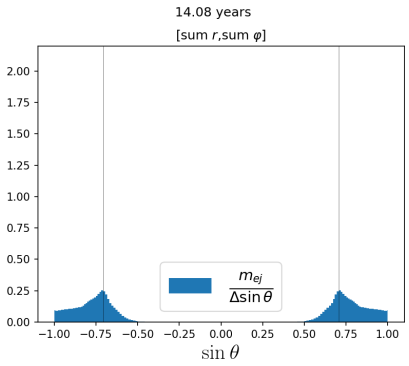

(b) $\alpha = 0.25$, $\beta = 0.817$

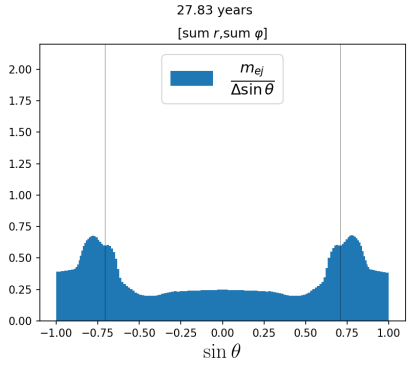

(c) $\alpha = 0.33$, $\beta = 0.588$

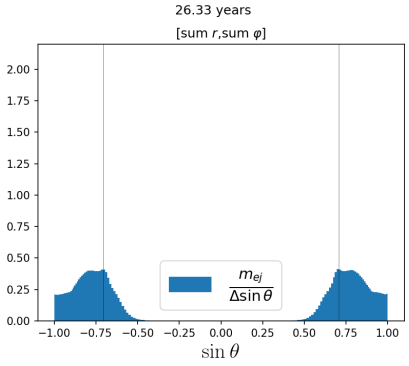

(d) $\alpha = 0.33$, $\beta = 0.817$

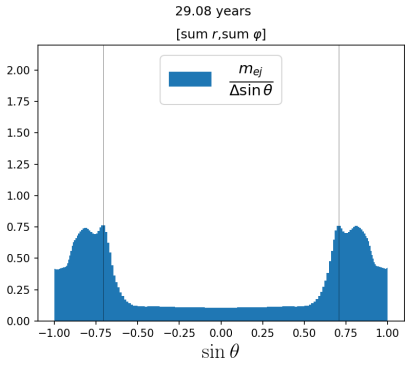

(e) $\alpha = 0.40$, $\beta = 0.817$

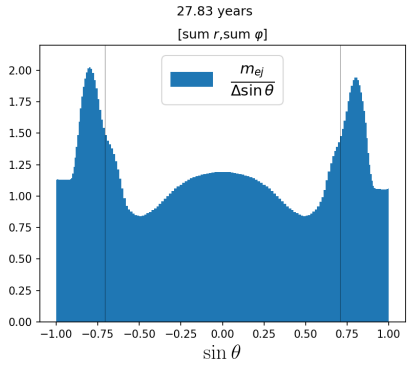

(f) $\alpha = 0.50$, $\beta = 0.588$

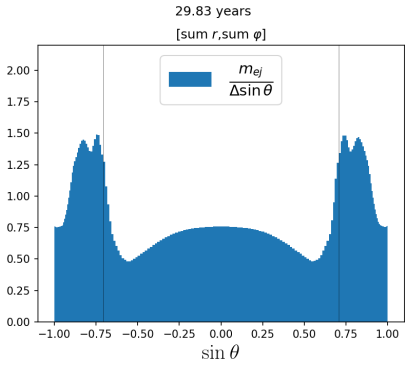

(g) $\alpha = 0.50$, $\beta = 0.817$

Figure 4.1: Final distribution of ejected mass as function of polar angle $\sin\theta$, which is zero at the equator. Bins correspond to cells of the simulation, so 192 bins are constant width in θ and not in $\sin\theta$. The ejected mass is divided by $\sin\theta$ to allow for "visual" integration. The black line corresponds to 45° angle.

Further in Table 4.1 we show total ejected mass for each simulated case. We can compare with Table 4.2 with results from T. Morris and Ph. Podsiadlowski 2006. For SN1987A ($\alpha = 0.40$, $\beta = 0.817$) we predict almost the same ejected mass. Though that seems to be just luck. For other ejected masses the prediction often differs by factor of two. For lower energies we have tendency to under estimate and for higher energies to over estimate in comparison. So far it is unclear what might be the reason behind this pattern.

α \ β	0.588	0.817
0.25	0.17	0.12
0.33	0.69	0.26
0.40	—	0.61
0.50	2.38	1.66

Table 4.1: Total ejected mass measured in $M_\odot$.

α \ β	0.588	0.817
0.25	0.21	0.18
0.33	0.42	0.38
0.40	0.63	0.58
0.50	1.00	0.89

Table 4.2: Total ejected mass measured in $M_\odot$ for comparison from T. Morris and Ph. Podsiadlowski 2006, table 3.

4.1 SN1987A Model

The values $\beta = 0.817$, $\alpha = 0.40$ correspond to SN1987A with assumption of solar masses 8 and 12 of initial stars, and initial orbital period of 10 years. As SN1987A is our main goal of study, we will focus on it further.

In Figure 4.2 we focus on density distribution roughly decade after the energy injection to observe the overall structure. In second subfigure we excise region that is gravitationally bound so that more of the color range is used for the ejected mass. From these we can see that mass is easily ejected at the polar region, and that it visibly amasses around the 45° latitude, forming the future ring.

For focus on dynamic evolution, video of mass, energy, escaped mass at each saved timestep of SN1987A model is shown in Attachment A.4.

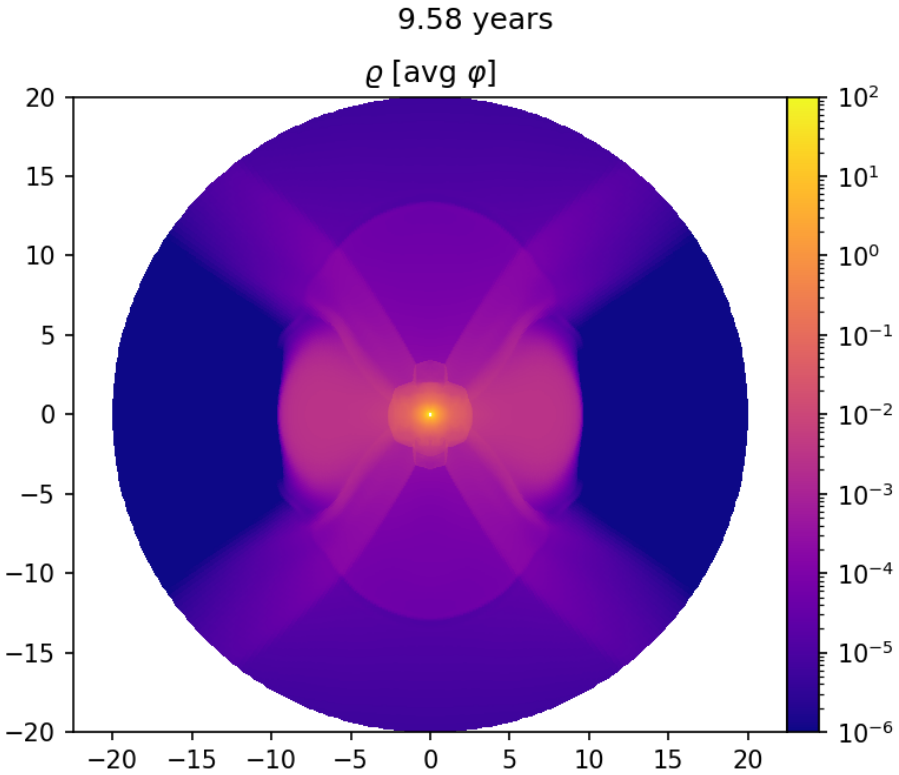

(a) Full density distribution.

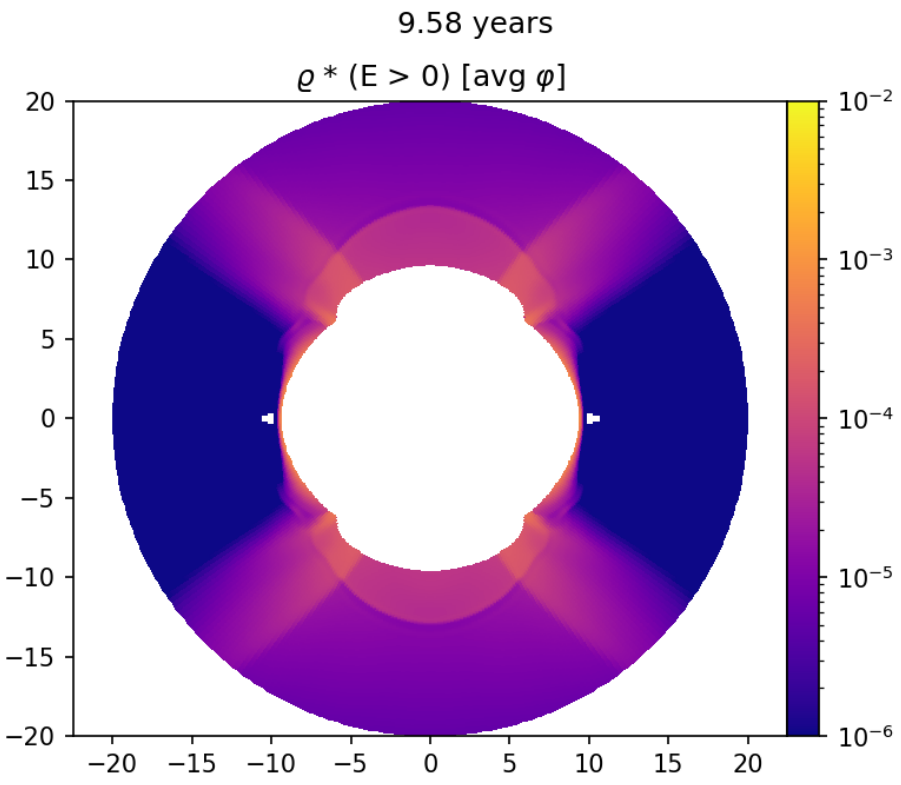

(b) Density distribution of only ejected mass, to focus on the rings.

Figure 4.2: Ejected mass in SN1987A model few years after energy injection.

Conclusion

Using mesh based hydrodynamic code Athena++ we simulated common envelope of binary merger to find ejection of mass which will result in non-equatorial rings of triple ring nebula observed around SN1987A. Using Athena++ we can predict the creation of non-equatorial rings, however we did achieve different results to T. Morris and Ph. Podsiadlowski 2006. Our peaks of ejected mass are at higher latitudes above 45°, while their are slightly under. We do agree on when mass is ejected in the equatorial region. We generally predict different total masses ejected by order of 2. For lower energies we have tendency to under estimate and for higher energies to over estimate in comparison. It is unclear what causes this pattern.

Athena++ unfortunately does not support self gravity in spherical coordinates. This might explain difference in latitude of ejected mass. It also means that a lot of values could not be computed directly from our model, and we had to use the direct values from T. Morris and Ph. Podsiadlowski 2006.

Since mesh based code is limited by the simulated region, we can only predict latitude distribution and total amount of ejected mass. It might be interesting to predict long term development of these ring. Which could be achieved by shifting the simulated region to follow the ring.

Bibliography

Gagnier, Damien and Ondřej Pejcha (2023). "Post-dynamical inspiral phase of common envelope evolution: Binary orbit evolution and angular momentum transport". In: *arXiv preprint arXiv:2302.00691*.

McCray, Richard and Claes Fransson (Sept. 2016). "The Remnant of Supernova 1987A". In: *araa* 54, pp. 19–52. DOI: 10.1146/annurev-astro-082615-105405.

Metzger, Brian D. and Ondřej Pejcha (July 2017). "Shock-powered light curves of luminous red novae as signatures of pre-dynamical mass-loss in stellar mergers". In: *Monthly Notices of the Royal Astronomical Society* 471.3, pp. 3200–3211. ISSN: 0035-8711. DOI: 10.1093/mnras/stx1768. eprint: https://academic.oup.com/mnras/article-pdf/471/3/3200/19515512/stx1768.pdf. URL: https://doi.org/10.1093/mnras/stx1768.

Morris, T and Ph Podsiadlowski (2009). "A binary merger model for the formation of the Supernova 1987A triple-ring nebula". In: *Monthly Notices of the Royal Astronomical Society* 399.2, pp. 515–538.

— (Jan. 2006). "Anisotropic mass ejection in binary mergers". In: *Monthly Notices of the Royal Astronomical Society* 365.1, pp. 2–10. DOI: 10.1111/j.1365-2966.2005.09645.x.

— (2007). "The Triple-Ring Nebula Around SN 1987A: Fingerprint of a Binary Merger". In: *Science* 315.5815, pp. 1103–1106. DOI: 10.1126/science.1136351. eprint: https://www.science.org/doi/pdf/10.1126/science.1136351. URL: https://www.science.org/doi/abs/10.1126/science.1136351.

NASA, ESA, and R. Kirshner (Harvard-Smithsonian Center for Astrophysics and Gordon and Betty Moore Foundation) and P. Challis (Harvard-Smithsonian Center for Astrophysics) (2017). *New image of SN1987A*. URL: https://esahubble.org/images/heic1704a/ (visited on 01/11/2024).

Podsiadlowski, Philipp (Sept. 1992). "THE PROGENITOR OF SN 1987A". In: *Publications of the Astronomical Society of the Pacific* 104.679, p. 717. DOI: 10.1086/133043. URL: https://dx.doi.org/10.1086/133043.

Springel, Volker (Dec. 2005). "The cosmological simulation code gadget-2". In: *Monthly Notices of the Royal Astronomical Society* 364.4, pp. 1105–1134. ISSN: 1365-2966. DOI: 10.1111/j.1365-2966.2005.09655.x. URL: http://dx.doi.org/10.1111/j.1365-2966.2005.09655.x.

Stone, James M. et al. (June 2020). "The Athena++ Adaptive Mesh Refinement Framework: Design and Magnetohydrodynamic Solvers". In: *The Astrophysical Journal Supplement Series* 249.1, p. 4. DOI: 10.3847/1538-4365/ab929b. URL: https://doi.org/10.3847/1538-4365/ab929b.

Sugerman, Ben E. K. et al. (July 2005). "A New View of the Circumstellar Environment of SN 1987A". In: *The Astrophysical Journal* 627.2, p. 888. DOI: 10.1086/430396. URL: https://dx.doi.org/10.1086/430396.

Toro, Eleuterio F (2009). *Riemann Solvers and Numerical Methods for Fluid Dynamics: A Practical Introduction*. Springer Science & Business Media.

A. Attachments

A.1 Code modifications - patches

Patches to the Athena++ repository. First one allows saving/exiting when specific condition is met — instead of only outputting at specific time intervals. Second one implements code averaging.
We use Athena++ version from February 3rd 2023 (specifically commit f16e877a35db84615d50e75db40fe066f3867ec7) as base code.

A.2 SN1987A problem generator

Problem generator to simulate SN1987A, belongs to ”src/pgen/” of Athena++ repository.

A.3 Input files

Input files for each simulation.

A.4 SN1987A 2D in time

Video of mass, energy, escaped mass at each saved timestep of simulation corresponding to SN1987A.